University of Nebraska - Lincoln
DigitalCommons@University of Nebraska - Lincoln

Biochemistry -- Faculty Publications | Biochemistry, Department of

2009

Mechanistic Details of Glutathione Biosynthesis Revealed by Crystal Structures of *Saccharomyces cerevisiae* Glutamate Cysteine Ligase

Ekaterina I. Biterova
University of Nebraska-Lincoln

Joseph J. Barycki
University of Nebraska-Lincoln, jbarycki2@unl.edu

Follow this and additional works at: http://digitalcommons.unl.edu/biochemfacpub

 Part of the Biochemistry Commons, Biotechnology Commons, and the Other Biochemistry, Biophysics, and Structural Biology Commons

Biterova, Ekaterina I. and Barycki, Joseph J., "Mechanistic Details of Glutathione Biosynthesis Revealed by Crystal Structures of *Saccharomyces cerevisiae* Glutamate Cysteine Ligase" (2009). *Biochemistry -- Faculty Publications*. 227.
http://digitalcommons.unl.edu/biochemfacpub/227

This Article is brought to you for free and open access by the Biochemistry, Department of at DigitalCommons@University of Nebraska - Lincoln. It has been accepted for inclusion in Biochemistry -- Faculty Publications by an authorized administrator of DigitalCommons@University of Nebraska - Lincoln.

PMCID: PMC2666596

THE JOURNAL OF BIOLOGICAL CHEMISTRY VOL. 284, NO. 47, pp. 32700–32708, November 20, 2009
© 2009 by The American Society for Biochemistry and Molecular Biology, Inc. Printed in the U.S.A.
Used by permission.

Mechanistic Details of Glutathione Biosynthesis Revealed by Crystal Structures of *Saccharomyces cerevisiae* Glutamate Cysteine Ligase*[S]

Received for publication, May 25, 2009, and in revised form, August 14, 2009 Published, JBC Papers in Press, September 2, 2009, DOI 10.1074/jbc.M109.025114

Ekaterina I. Biterova and Joseph J. Barycki[1]

From the Department of Biochemistry and the Redox Biology Center, University of Nebraska, Lincoln, Nebraska 68588-0664

Glutathione is a thiol-disulfide exchange peptide critical for buffering oxidative or chemical stress, and an essential cofactor in several biosynthesis and detoxification pathways. The rate-limiting step in its *de novo* biosynthesis is catalyzed by glutamate cysteine ligase, a broadly expressed enzyme for which limited structural information is available in higher eukaryotic species. Structural data are critical to the understanding of clinical glutathione deficiency, as well as rational design of enzyme modulators that could impact human disease progression. Here, we have determined the structures of *Saccharomyces cerevisiae* glutamate cysteine ligase (ScGCL) in the presence of glutamate and $MgCl_2$ (2.1 Å; $R = 18.2\%$, $R_{free} = 21.9\%$), and in complex with glutamate, $MgCl_2$, and ADP (2.7 Å; $R = 19.0\%$, $R_{free} = 24.2\%$). Inspection of these structures reveals an unusual binding pocket for the α-carboxylate of the glutamate substrate and an ATP-independent Mg^{2+} coordination site, clarifying the Mg^{2+} dependence of the enzymatic reaction. The ScGCL structures were further used to generate a credible homology model of the catalytic subunit of human glutamate cysteine ligase (hGCLC). Examination of the hGCLC model suggests that post-translational modifications of cysteine residues may be involved in the regulation of enzymatic activity, and elucidates the molecular basis of glutathione deficiency associated with patient hGCLC mutations.

Glutathione, γ-glutamylcysteinyl glycine, is a low molecular weight thiol, central to maintenance of redox homeostasis. Among its normal functions are the scavenging of reactive oxygen and nitrogen species (1), storage and transport of cysteine (2, 3), leukotriene, and prostaglandin biosynthesis (4, 5), and regulation of enzyme activity via reduction of disulfide bonds and glutathionylation (6, 7). Disruption of glutathione metabolism is associated with the progression of AIDS, cancer, and neurodegenerative conditions such as Parkinson and Alzheimer disease (8–12). Polymorphisms that reduce activity of glutamate cysteine ligase (GCL),[2] the first and rate-limiting enzyme in *de novo* synthesis of glutathione, are correlated with reduced glutathione levels in patients with hemolytic anemia, schizophrenia and other neurological disorders (13–16). Given its importance both in normal and disease states, there is considerable interest in the development of novel compounds that could be used to modulate intracellular glutathione levels, potentially via GCL.

Glutathione is synthesized from its three constituent amino acids by consecutive action of two cytosolic ATP-dependent enzymes: GCL and glutathione synthetase (17). GCL catalyzes the conjugation of the γ-carboxyl group of L-glutamate to the amino group of L-cysteine (17). The proposed catalytic mechanism proceeds via phosphorylation of the γ-carboxylate of L-glutamate by ATP (18–20). The α-amino group of L-cysteine acts as a nucleophile, attacking the γ-glutamyl phosphate intermediate to produce γ-glutamylcysteine. This dipeptide is then coupled in an analogous fashion to glycine by glutathione synthetase to generate glutathione. As the committed step of glutathione biosynthesis, GCL activity is regulated by L-cysteine availability (21), feedback inhibition by glutathione (22), and transcriptional and post-translational regulation (23).

Based on sequence analysis, three distinct groups of GCL have been identified. Groups 1 and 3 are comprised of bacterial and plant orthologues (24). Recently, x-ray crystal structures of *Escherichia coli* (Group 1) (25) and *Brassica juncea* (Group 3) (26) GCL were described, providing the first structural insights into γ-glutamylcysteine synthesis. However, low sequence identity (<10%) between enzymes of different groups has precluded translation of these structural data into a detailed understanding of the molecular features of enzymes in Group 2, the class that encompasses yeast and mammalian GCL. One structurally unique feature of several Group 2 GCL is the potential for higher order regulation imposed by their existence in reversible heterodimeric complexes of a catalytic (GCLC) and a modulatory subunit (GCLM) (17). To circumvent the inherent challenges associated with structural studies of the complex, we selected the monomeric *Saccharomyces cerevisiae* GCL (ScGCL), a member of a unique subclass of Group 2 GCL, as a model system for higher eukaryotic GCL. Although ScGCL differs from human GCLC in its oligomeric state, the two enzymes share ~45% sequence identity (24).

* This work was supported, in whole or in part, by National Institutes of Health Grant Number 1R01 GM077289 (to J. J. B.).

The atomic coordinates and structure factors (codes 3IG5 and 3IG8) have been deposited in the Protein Data Bank, Research Collaboratory for Structural Bioinformatics, Rutgers University, New Brunswick, NJ (http://www.rcsb.org/).

[S] The on-line version of this article (available at http://www.jbc.org) contains supplemental Figs. S1 and S2.

[1] To whom correspondence should be addressed: Dept. of Biochemistry and Redox Biology Center, University of Nebraska, 1901 Vine St., Lincoln, NE 68588-0664. Tel.: 402-472-9307; Fax: 402-472-7842; E-mail: jbarycki2@unl.edu.

[2] The abbreviations used are: GCL, glutamate cysteine ligase; DTT, dithiothreitol; r.m.s.d., root mean-square deviation; AMP-PNP, adenosine 5′-(β,γ-imido)triphosphate; PDB, Protein Data Bank; MES, 2-(*N*-morpholino)ethanesulfonic acid; PEG, polyethyleneglycol.

In the current study, we present the crystal structures of ScGCL in complex with glutamate and Mg^{2+}, as well as in the presence of glutamate, Mg^{2+}, and ADP. Examination of these structures provides considerable insights into catalysis and reveals a unique coordination at the α-carboxylate of the glutamate substrate. Based on the ScGCL structure, a homology model of human GCLC was generated to investigate the molecular details of several human patient mutations with reduced activity, and to aid in the design of novel modulators of GCL activity.

EXPERIMENTAL PROCEDURES

Generation of ScGCL Expression Construct—A predicted open reading frame in the *S. cerevisiae* genome (KEGG Data Base Entry YJL101C) (27, 28) was amplified by the polymerase chain reaction using *S. cerevisiae* genomic DNA (American Type Culture Collection) as a template. Designed primers contained SpeI (forward) and SalI (reverse) restrictions sites. The resultant 2-kb product was digested with the relevant enzymes and ligated into a complementarily digested pET-21a(+) expression vector (Novagen; NheI and SalI), thus incorporating a C-terminal histidine tag. The expression construct was sequenced at the Genomics Facility of University of Nebraska (Lincoln, NE) and confirmed to be identical to the YJL101C sequence.

Protein Expression and Purification—The ScGCL construct was used to transform *Escherichia coli* Rosetta^{TM}2(DE3) pLysS cells (Novagen). Cells were grown in 2xYT medium containing 100 μg ml^{-1} ampicillin and 34 μg ml^{-1} chloramphenicol at 37 °C, and ScGCL production was induced by the addition of 500 μM isopropyl-1-thio-β-D-galactopyranoside once the cells reached an A_{600} of 0.6. After induction, cultures were grown for 4 h at 30 °C. Cells were harvested by centrifugation (20 min, 8000 $\times$ *g*, 4 °C) and stored at −80 °C. Frozen cell pellets were thawed, resuspended in lysis buffer (50 mM sodium phosphate buffer, pH 8.0, 300 mM NaCl, 0.2 mM protease inhibitor, 10 mM imidazole), and disrupted by sonication. Following centrifugation to remove cellular debris (30 min, 20,000 $\times$ *g*, 4 °C), the supernatant was loaded onto a HisTrap Chelating HP Column (GE Healthcare) equilibrated with lysis buffer. The column was washed to baseline (A_{280}), and the remaining bound proteins were eluted using a linear imidazole gradient (10–250 mM). Fractions containing ScGCL were pooled, concentrated, and loaded onto a Sephacryl 200 gel filtration column (16 $\times$ 600 mm) equilibrated with 50 mM Tris-HCl, pH 7.4, 300 mM NaCl, and 2 mM DTT. Samples containing ScGCL were pooled and dialyzed against crystallization buffer (20 mM Tris-HCl, pH 7.4, 2 mM DTT). The enzyme was concentrated to 12 mg ml^{-1} using an Amicon ultrafiltration device (Stirred cell 8050, 10-kDa cutoff), flash-frozen in liquid nitrogen, and stored at −80 °C. The enzyme concentration was determined by absorbance (280 nm) using a calculated extinction coefficient (29) of 105,200 M^{-1} cm^{-1}.

Characterization of ScGCL—ScGCL was examined by analytical gel filtration chromatography on a Superdex 200 HR 10/30 column (GE Healthcare, equilibrated with 20 mM Tris, pH 7.4, 150 mM NaCl, 2 mM DTT). Molecular weight determinations were made by comparison with the following standards: thyroglobulin, 699 kDa; ferritin, 416 kDa; catalase, 219 kDa; aldolase, 176 kDa; albumin, 67 kDa; ovalbumin, 47 kDa; chymotrypsinogen A, 20 kDa; RNase A, 15 kDa (GE Healthcare). Enzymatic activity was measured in the presence of 20 mM L-glutamate, 10 mM L-cysteine, 5 mM ATP, and 50 mM $MgCl_2$, using an indirect assay that couples ADP production to NADH oxidation (30).

Structure Determination of ScGCL—Initial crystallization screening was performed by the sitting-drop vapor-diffusion method using sparse matrix crystal screens (Qiagen). Crystals of ScGCL (7 mg/ml) were ultimately grown at 18 °C out of a solution of 12% (w/v) PEG 400, 100 mM MES, pH 6.8, and reached the dimensions 0.15 $\times$ 0.15 $\times$ 0.15 mm. Once suitable crystallization conditions were established, several complexes were co-crystallized as indicated below.

An extensive search of potential heavy metal derivatives was conducted and a derivative suitable for phasing was identified. ScGCL was incubated with 1 mM trimethyl lead acetate, 5 mM L-glutamate, 5 mM ATP, and 20 mM $MgCl_2$ and co-crystallized. Crystals were transferred into an appropriate stabilizing solution, containing 100 mM MES, pH 6.8, 5 mM ATP, 5 mM L-glutamate, 20 mM $MgCl_2$, and 30% PEG 400 and vitrified in the cryostream (X-Stream cooling system; Rigaku) (31). Diffraction data were collected using radiation produced by a Rigaku MicroMax-007 x-ray generator fitted with confocal blue optics and an R-axis IV^{++} image plate system (λ = 1.54 Å; 100 K). Data were processed with the HKL2000 software package (32). The structure of ScGCL derivatized with trimethyl lead acetate was solved using experimental phases determined by single wavelength anomalous diffraction utilizing the PHENIX software suite (33). A readily interpretable electron density map was obtained, and automated model building was employed. The initial model contained a single Pb^{2+} bound at the enzyme active site. Since the Pb^{2+} occupied one of the three Mg^{2+} binding sites, M2 (see below), this initial model was used only as a search probe for subsequent ScGCL complex structure determinations.

To examine the structural basis of catalysis and substrate recognition, several ScGCL complexes were pursued. ScGCL was incubated with 5 mM L-glutamate, 5 mM AMP-PNP, 5 mM L-cysteine, and 20 mM $MgCl_2$ or 5 mM L-glutamate, 5 mM ADP, 5 mM L-cysteine, and 20 mM $MgCl_2$ and both complexes were crystallized. Crystals were transferred to a suitable cryosolution (30% PEG 400, 100 mM MES, pH 6.8, and the appropriate ligands) and then stored in liquid nitrogen. Diffraction data (λ = 0.9 Å; 100 K) were collected on Beamline 14-BM-C of BioCARS at Argonne National Laboratory's Advanced Photon Source and were processed with the HKL2000 software package (32).

The structures were solved by molecular replacement within the PHENIX software suite (33) using the initial ScGCL model as a probe. Iterative rounds of model building and refinement were carried out using Coot (34) and Refmac5 (35) respectively. As the protein models neared completion, water molecules obeying proper hydrogen-bonding constraints with electron density greater than 1.0 σ on a $2F_o–F_c$ map and 4.0 σ on an $F_o–F_c$ map were also included in the final structure. Model geometry was monitored using MOLPROBITY (36), and fig-

TABLE 1
Data collection and refinement statistics

	Glu/ADP/Mg^{2+}/Pb	Glu/Mg^{2+}	Glu/ADP/Mg^{2+}	Glu/ADP/Mn^{2+}
Data collection				
PDB Accession Code	NA	3IG5	3IG8	NA
λ	1.54Å	0.90 Å	0.90 Å	1.54Å
Temperature (K)	100	100	100	100
Space group	$P4_32_12$	$P4_32_12$	$P4_32_12$	$P4_32_12$
Cell dimensions				
a, *b*, *c* (Å)	117.7, 117.7, 165.7	117.4, 117.4, 165.4	117.8, 117.8, 165.4	117.7, 117.7, 165.7
Resolution (Å)	50-2.3 (2.38-2.30)[a]	50-2.1 (2.18-2.10)	50-2.7 (2.75-2.70)	50-2.9 (2.95-2.90)
R_{merge} (%)	8.4 (63.7)	6.9 (57.8)	9.6 (72.7)	11.3 (71.5)
Mean I/σI	40.2 (3.9)	20.9 (1.8)	19.4 (2.3)	12.1 (1.8)
Completeness (%)	99.9 (100)	97.5 (96.1)	94.7 (96.0)	99.6 (99.7)
Redundancy	17.4 (16.1)	4.5 (3.6)	7.0 (5.8)	5.5 (5.3)
Refinement				
Resolution (Å)		32-2.1 (2.15-2.10)	34-2.7 (2.76-2.70)	
No. reflections		54225	27023	
R_{work}/R_{free} (%)		18.2/21.9 (26.2/29.8)	19.0/24.2 (22.8/29.7)	
No. atoms		5869	5621	
Protein		5490	5461	
Ligand/ion		51	50	
Water		328	110	
Average B-factors (Å^2)		38.0	43.2	
Protein		37.7	43.4	
Ligand/ion		54.1	51.5	
Water		39.7	36.9	
R.m.s. deviations from ideal				
Bond lengths (Å)		0.019	0.019	
Bond angles (°)		1.68	1.88	
Ramachandran statistics				
Favored		96.7%	94.0%	
Allowed		99.7%	99.0%	

[a] Values in parentheses are for highest-resolution shell.

ures were produced using Chimera (37). To validate the location of the metal binding sites, ScGCL was crystallized in the presence of 5 mM L-glutamate, 5 mM ADP, 5 mM L-cysteine, and 20 mM $MnCl_2$. Diffraction data were collected using radiation produced by a Rigaku MicroMax-007 x-ray generator fitted with confocal blue optics and an R-axis IV^{++} image plate system (λ = 1.54 Å; 100 K). Data were processed with the HKL2000 software package (32) and an anomalous difference map was calculated.

RESULTS

Characterization of ScGCL—ScGCL was purified from *E. coli* with a specific activity of ~10 μmoles/min/mg of protein, comparable to other glutamate cysteine ligases. Both analytical gel filtration chromatography as well as sedimentation velocity experiments indicated that ScGCL was likely a monomer in solution (data not shown). As discussed below, a single polypeptide chain is contained within the asymmetric unit of ScGCL crystals, and relatively modest interactions between crystallographically related molecules are observed, consistent with a monomeric enzyme. Although GCL is typically a heterodimer comprised of a catalytic subunit and a modifier subunit in higher eukaryotes (Group 2), phylogenetic analysis suggests that members of the hemiascomycete class of fungi do not have a modifier subunit and that ScGCL likely functions as a monomer *in vivo*.

Overall Structure of ScGCL—Phase information was obtained using single wavelength anomalous diffraction data collected from a crystal of ScGCL derivatized with trimethyl lead acetate (Table 1). The PHENIX software suite (33) was used to identify the positions of one lead (coincident with the M2 binding site described below) and each of the ordered 22 sulfur atoms in the final model (8 of 9 cysteine residues; 14 of 15 methionine residues), and to calculate an initial experimentally phased map. ScGCL crystals have a calculated solvent content of ~65% and density modification in PHENIX significantly improved the experimental phases (supplemental Fig. S1). Automated chain tracing resulted in a model that contained ~90% of the ScGCL sequence. This initial model was used for subsequent structure determinations of the ScGCL complexes by molecular replacement. ScGCL was also crystallized in the presence of L-glutamate, AMP-PNP, cysteine, and Mg^{2+}, or L-glutamate, ADP, cysteine, and Mg^{2+}. Data sets were collected to 2.1 Å and 2.7 Å, respectively (Table 1). However, convincing electron density was not observed for either AMP-PNP or cysteine. Refinement statistics for the final ScGCL models, corresponding to residues 2 through 676, are provided in Table 1. The ScGCL/Glu/Mg^{2+} and the ScGCL/Glu/Mg^{2+}/ADP complexes have 99.7 and 99.0% of residues, respectively, in the allowed region of the Ramachandran plot as assessed by MOLPROBITY (36).

A single polypeptide chain is contained within the asymmetric unit of ScGCL crystals, and relatively modest interactions between crystallographically related molecules are observed, consistent with a monomeric enzyme. The ScGCL fold (Fig. 1) shows strong structural similarity to other members of the ATP-grasp superfamily, and has a core β-sheet comprised of six anti-parallel β-strands surrounded by α-helices. The N terminus of the protein defines a lip of the active site, which is situated in a central cavity of the protein. Despite low sequence identity (~10%), the core fold of the ScGCL structure is similar

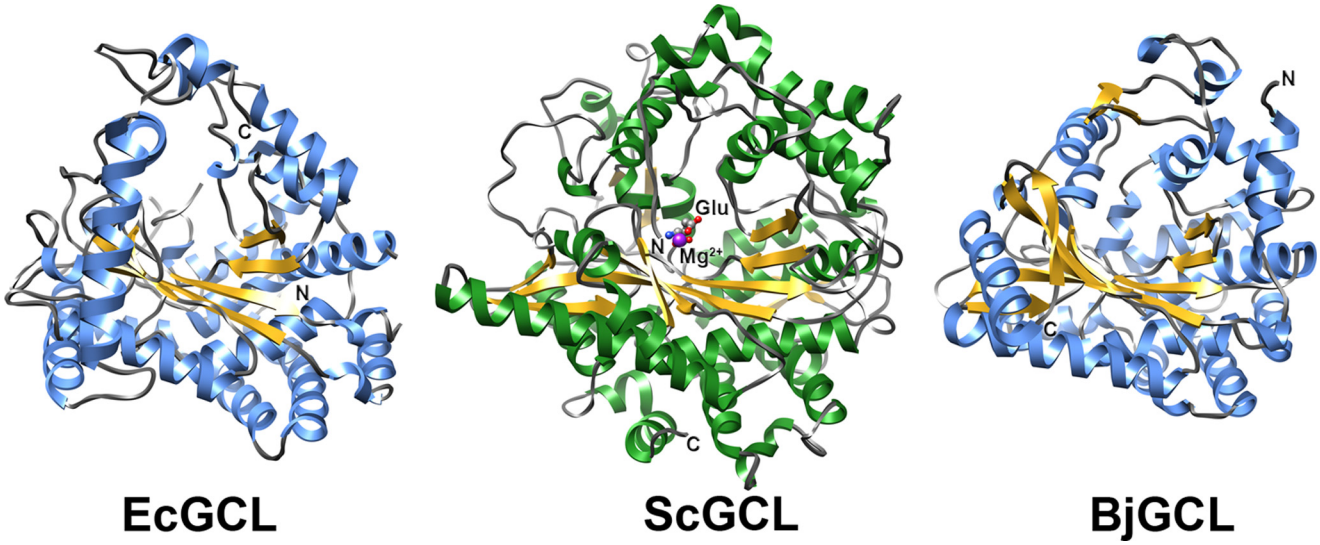

FIGURE 1. **Ribbon representation of the recombinant ScGCL crystal structure.** A functionally active ScGCL monomer (~78 kDa) is contained in the asymmetric unit (*center*). The core β-sheet is colored in *yellow*, α-helical elements in *green*, and loop regions in *gray*. The glutamate substrate is shown in ball and stick representation with carbon atoms colored in *gray*, oxygen atoms in *red*, and nitrogen atoms in *blue*. A bound Mg^{2+} is represented by a *purple sphere*, and the N- and C-terminal residues are indicated. For comparison, the ribbon representations of the previously determined *E. coli* (25) (2D32) and *B. juncea* (26) (2GWD) GCL structures are shown with β-strands colored in *yellow*, α-helices in *blue*, and loop regions in *gray*.

to those of the previously determined *E. coli* (25) (2D32; rmsd 2.3 Å for 266 C_α atoms) and *B. juncea* (26) (2GWD; r.m.s.d. 2.0 Å for 321 C_α atoms) GCL structures with several differences of note (Fig. 1). The larger ScGCL structure (678 residues), relative to the bacterial (518 residues) and plant (514 residues) homologues, contains three additional short β-sheets formed by anti-parallel β-strands, as well as extended α-helical and loop regions.

An intriguing feature of the structure is a cysteine residue, Cys-70, that appears to be oxidized to sulfenic acid (supplemental Fig. S2). As discussed below, there are several prominent cysteine residues in ScGCL, suggesting that cysteine oxidation and/or additional post-translational modifications may play an important regulatory role. In support of this hypothesis, previous studies have shown that H_2O_2 increases the enzymatic activity of GCL (38, 39). However, the mechanism of this activation was not demonstrated, and additional studies are needed to clarify the functional significance of Cys-70 oxidation.

Identification of the L-glutamate Binding Site and an ATP-independent Bound Mg^{2+} Cofactor—In the ScGCL structure, L-glutamate is bound in the extended conformation in the interior of the funnel-shaped active site cavity (Fig. 2*A*), with the side chains of Arg-313 and Tyr-362 positioning the α-carboxylate of the glutamate substrate. The α-amino group of glutamate is within hydrogen bond distance of the backbone carbonyl of Cys-264, the γ-carboxylate of Glu-52, and a bound water molecule, which is positioned by the carboxylate of Glu-96 and the backbone carbonyl of Met-262. The γ-carboxylate of the glutamate substrate occupies one of the coordination sites of an interesting Mg^{2+} cofactor (discussed below) and is in close proximity to the side chain of Arg-472. An additional feature of the glutamate-binding pocket is Cys-266, which is stacked 3.2 Å below the α-carboxylate carbon atom.

Interestingly, despite the absence of ATP, electron density was also observed for an octahedrally coordinated Mg^{2+} at the enzyme active site. The bound Mg^{2+} is within 2.2 Å of two active site glutamate residues, Glu-52 and Glu-103, and near the γ-carboxylate of the glutamate substrate (Fig. 2*B*). A fourth glutamate, Glu-96, and an ordered water molecule, positioned by Glu-50, are also located adjacent to the bound magnesium ion (2.6 Å and 2.4 Å, respectively). A water molecule occupies the final coordination site (1.9 Å), but its corresponding electron density is poorly defined. As discussed below, binding of ADP is accompanied by the formation of two additional magnesium binding sites.

Identification of the ADP Binding Site and Examination of the Metal Coordination—Since convincing electron density was not observed for the non-hydrolyzable ATP analogue in the active site of the initial ScGCL/Glu/Mg^{2+} complex, a second data set was collected in which ADP replaced AMP-PNP (Table 1). In the ScGCL/Glu/Mg^{2+}/ADP complex, ADP is largely solvent-exposed, with its adenine ring on the outer edge of the active site pocket, and its β-phosphate positioned near the γ-carboxylate of the bound glutamate substrate. Relatively few hydrogen bonds anchor the adenosine portion of the molecule (Fig. 3*A*). The N6 atom of the adenine ring is within hydrogen bond distance of the side chain of Gln-272. The 2′-hydroxyl group of the ribose ring interacts with the backbone carbonyl of Pro-106 via a bridging water molecule, and the 3′-hydroxyl group is within hydrogen bond distance of the backbone carbonyl of Asp-49. In addition, the 3′-hydroxyl group forms a hydrogen bond with a structurally conserved water molecule that is held in place by hydrogen bonds to the backbone carbonyl of Gly-48 and the side chains of Thr-270 and Glu-50. Lys-451, via bridging water molecules, appears to contribute to the orientation of the β-phosphate. However, the most striking interactions of this terminal phosphate are with two bound magnesium ions, M2 and M3 (Fig. 3).

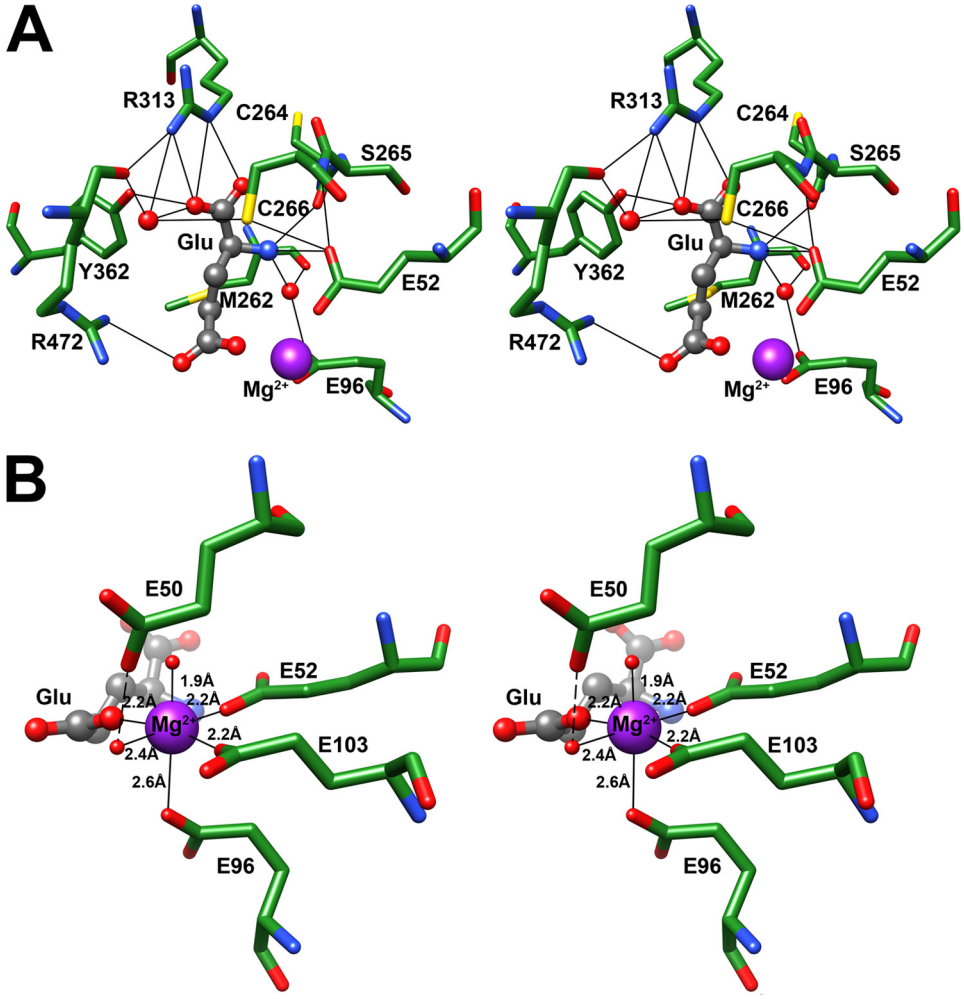

FIGURE 2. **Stereodiagrams of the glutamate and Mg^{2+} binding sites.** The refined model of ScGCL in complex with glutamate and Mg^{2+} is depicted with pertinent active site residues shown in *stick representation*. Oxygen atoms are shown in *red*, nitrogen atoms in *blue*, sulfur atoms in *yellow*, and Mg^{2+} in *purple*. Carbon atoms are colored *green* in ScGCL and *gray* in the bound glutamate (shown in *ball and stick* representation). *Panel A*, potential hydrogen bonds between the bound glutamate substrate and ScGCL are indicated as *solid black lines*. Of particular interest is the proximity of the side chain of Cys-266 to the α-carboxylate of the bound glutamate. *Panel B*, the coordination of the bound M1 Mg^{2+} is illustrated with relevant interatomic distances indicated (*solid lines*). A potential hydrogen bond between a bound water molecule and the side chain of Glu-50 is designated by a *dashed line*.

Three bound metal ions were identified in the ScGCL/Glu/Mg^{2+}/ADP complex. The first metal binding site, M1, is comparable to the Mg^{2+} site identified in the initial ScGCL/Glu/Mg^{2+} complex. As before, the γ-carboxylates of Glu-52, Glu-103, and the glutamate substrate are within 2.2 Å of the metal. The side chain carboxylate of Glu-96 moves ~0.4 Å closer to the M1 metal site, and is also positioned ~2.2 Å from the bound Mg^{2+}. The two bound water molecules seen in the ScGCL/Glu/Mg^{2+} complex are absent in the ScGCL/Glu/Mg^{2+}/ADP complex. The binding of ADP results in the formation of two additional Mg^{2+} sites. The second site, M2, is created by the side chain oxygen atoms of Gln-268, Glu-470, and Glu-50 as well as an oxygen atom from the β-phosphate of ADP. Similarly, the third Mg^{2+}, M3, is coordinated by side chain oxygen atoms of Glu-103 and Glu-50 as well as an oxygen atom from the β-phosphate of ADP. The γ-phosphate of ATP would likely bind adjacent to the γ-carboxylate of the glutamate substrate, positioned optimally for catalysis by the three bound Mg^{2+} ions.

To confirm the placement of the three Mg^{2+} in the final ScGCL/Glu/Mg^{2+}/ADP complex model, a comparable data set in which the Mg^{2+} was replaced with Mn^{2+} during crystallization was collected (Table 1). Mn^{2+} has been shown to support catalysis by glutamate cysteine ligase (40) and has a significant anomalous signal at a wavelength of 1.54 Å (K edge at 1.89 Å). An anomalous difference map was calculated and examined (Fig. 3*B*). Three major peaks (>8σ) were identified, presumably corresponding to each of the three bound Mn^{2+} ions, which superimpose well on the three bound Mg^{2+} in the final ScGCL/Mg^{2+}/ADP/Glu complex model. The interatomic Mg^{2+} distances are 4.75 Å between M1 and M2, 4.06 Å between M2 and M3, and 3.36 Å between M1 and M3.

Homology Modeling of the Human Glutamate Cysteine Ligase Catalytic Subunit (hGCLC)—There have been several published attempts to generate a homology model of hGCLC using either the functionally related *T. thermophilus* glutamyl-tRNA synthetase or *E. coli* YbdK (41, 42). However, comparison of these models with the ScGCL structure reported herein shows significant structural dissimilarities, revealing the limitations of models derived from such distant homologues. Using the PDB-Viewer software package (43), a homology model of hGCLC was generated (Fig. 4) that retains the overall fold of ScGCL. Several regions of the hGCLC sequence (residues 210–223, 312–324, 490–507) have low sequence identity to ScGCL. These regions correspond to poorly defined surface loops (shown in green) in the final hGCLC model. Comparison of the active sites of the hGCLC homology model and the ScGCL structure indicates that the two enzymes have nearly identical active site architectures with almost complete conservation of side chain functionality. A remarkable feature of the hGCLC model is that the fourteen cysteine residues of the protein are located primarily in a single hemisphere of the protein. Several of these solvent-exposed cysteine residues may be important for the post-translational regulation of hGCL activity. Atomic coordinates and structure factors have been deposited in the PDB under accession codes 3IG5 and 3IG8.

DISCUSSION

Glutathione is a vital cellular reductant and a critical biological cofactor. GCL catalyzes the rate-limiting step in its biosyn-

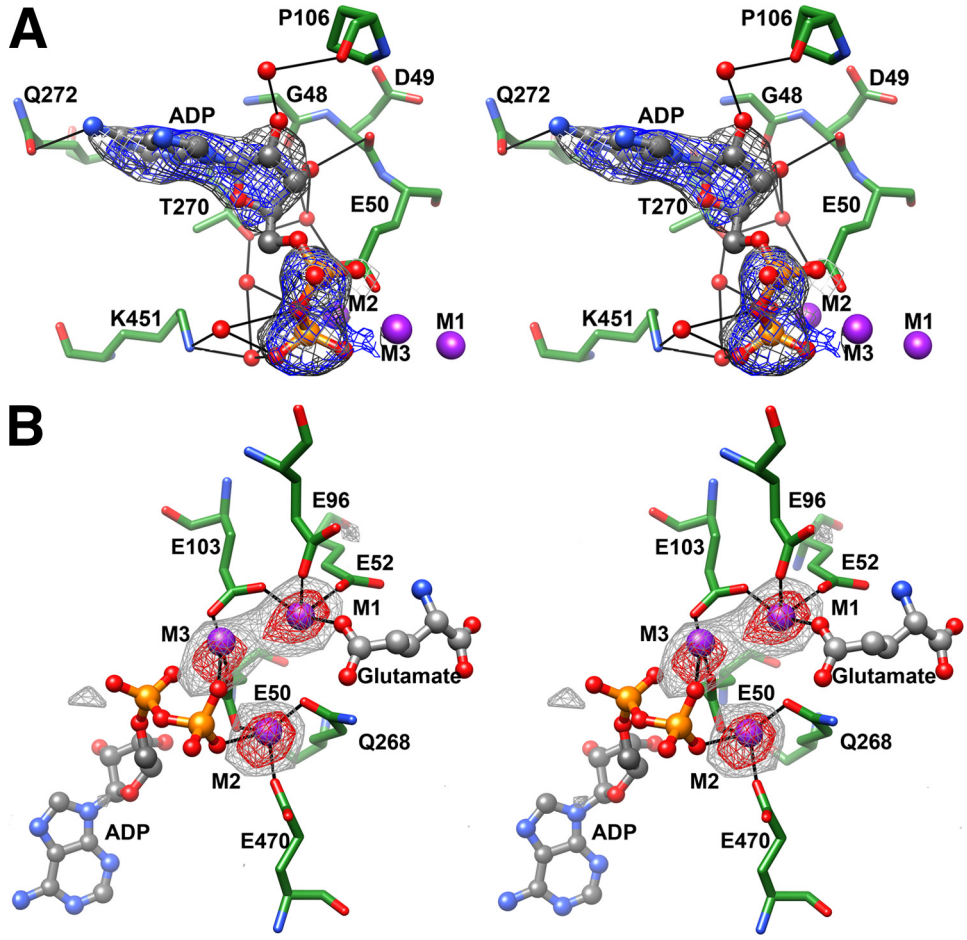

FIGURE 3. **Stereodiagrams of the ADP and Mg^{2+} binding sites.** The refined model of ScGCL in complex with ADP, glutamate, and Mg^{2+} is depicted with pertinent active site residues in *stick* representation. Bound ligands are shown in *ball and stick* representation, and atoms are colored as in Fig. 2, with the addition of phosphorus, shown in *orange*. *Panel A*, shown are the calculated electron density maps after several rounds of refinement, but prior to inclusion of ADP in the model. The relevant $2F_o–F_c$ electron density is contoured at 1.0 σ and illustrated in *gray*. Positive and negative peaks in the $F_o–F_c$ difference map, contoured at 4.0σ, are shown in *blue* and *red*, respectively. Potential hydrogen bonds between ADP and ScGCL are indicated as *solid black lines*. The adenine ring is located at the top of the active site cavity, near the surface of the protein. The β-phosphate is positioned in part through interactions with Lys-451 via bridging water molecules. *Panel B*, the anomalous difference map calculated using diffraction data from the corresponding Mn^{2+} complex supports the location of each of the three bound Mg^{2+} ions in the final ScGCL model. The relevant anomalous difference peaks are contoured at 3.0 σ (*gray*) and 6.0 σ (*red*). The coordination of each of the three Mg^{2+} ions is shown as *solid black lines* that correspond to atom/metal pairs with interatomic distances of ~2.2 Å.

thesis and is an essential enzyme in mammalian systems (17). Strikingly, the ScGCL structure maintains the overall fold observed in the *E. coli* (Group 1) (25) and the *B. juncea* (Group 3) (26) enzymes (Fig. 1), suggesting that the three classes of enzymes arose from a common ancestor. Conservation of side chain functionality is observed within each active site even though the three enzymes share <10% sequence identity. For example, the M2 binding site of ScGCL formed by Glu-50, Gln-268, and Glu-470 (Fig. 3*B*) is similarly comprised of Glu27, His-150, and Glu-328 in the *E. coli* enzyme. This proposed active site conservation is further supported by mutagenesis studies of GCL from other species. Arg-313 in ScGCL forms hydrogen bonds with the α-carboxylate of the glutamate substrate. In *Trypanosoma brucei* GCL, mutation of the equivalent residue, Arg-366, to Ala increased its K_d for glutamate >160-fold (44). Similarly, mutation of Arg-491 (Arg-472 in ScGCL; Fig. 2*B*) affected K_m for glutamate modestly but decreased enzymatic activity of *T. brucei* GCL 70-fold (44), suggesting a direct role in catalysis.

A unique feature of the ScGCL active site is the placement of a cysteine residue, Cys-266, proximal to the α-carboxylate of the glutamate substrate (Fig. 4). This residue is highly conserved among higher eukaryotic GCL and its importance has been examined in a number of homologues (45, 46). Previous modeling studies of human GCL indicated that Cys-249, analogous to Cys-266 of ScGCL, was located in the periphery of the enzyme active site and not directly involved in substrate binding or catalysis (41). However, our model of hGCLC suggests that Cys-249 is located at the base of the glutamate-binding pocket. Further support for an active role is provided by mutational analysis of hGCLC in which Cys-249 was substituted with a glycine, resulting in a 10-fold reduction in enzymatic activity (47). Similarly, a C248A/C249A double mutant in the mouse GCL catalytic subunit resulted in a >4-fold reduction in enzymatic activity (48). Mutagenesis studies to examine the precise role of Cys-266 in ScGCL function using both *in vitro* and *in vivo* approaches are ongoing.

Despite its inclusion in crystallization trials, cysteine was not observed in either ScGCL complex. Examination of the ScGCL structure suggests a possible cysteine binding site adjacent to the bound glutamate substrate. Glu-96 likely forms a hydrogen bond with the α-amino group of the incoming cysteine residue. The side chains of Trp-445 and Arg-196 both point into the putative L-cysteine binding site, and either residue may form a hydrogen bond with the α-carboxylate of L-cysteine. A hydrophobic pocket, lined by Tyr-97, Phe-197, Leu-200, Met-258, and Met-262, could accommodate the sulfhydryl group. Additional studies of ScGCL are required to ascertain the precise recognition mechanisms critical for cysteine binding.

Conflicting catalytic mechanisms have been postulated for GCL. Early studies using the rat homologue suggested a quaternary complex in which ATP/Mg^{2+} binds first, followed by L-glutamate and L-cysteine in random order (20, 49). Recent comprehensive reports support a random ter-reactant mechanism in the *T. brucei* and *Arabidopsis thaliana* enzymes (46, 50). Examination of the reported ScGCL structures suggests that the active site is large enough to accommodate ATP, Mg^{2+}, glutamate, and cysteine simultaneously. However, the glutamate-binding pocket would be completely obstructed if ATP/

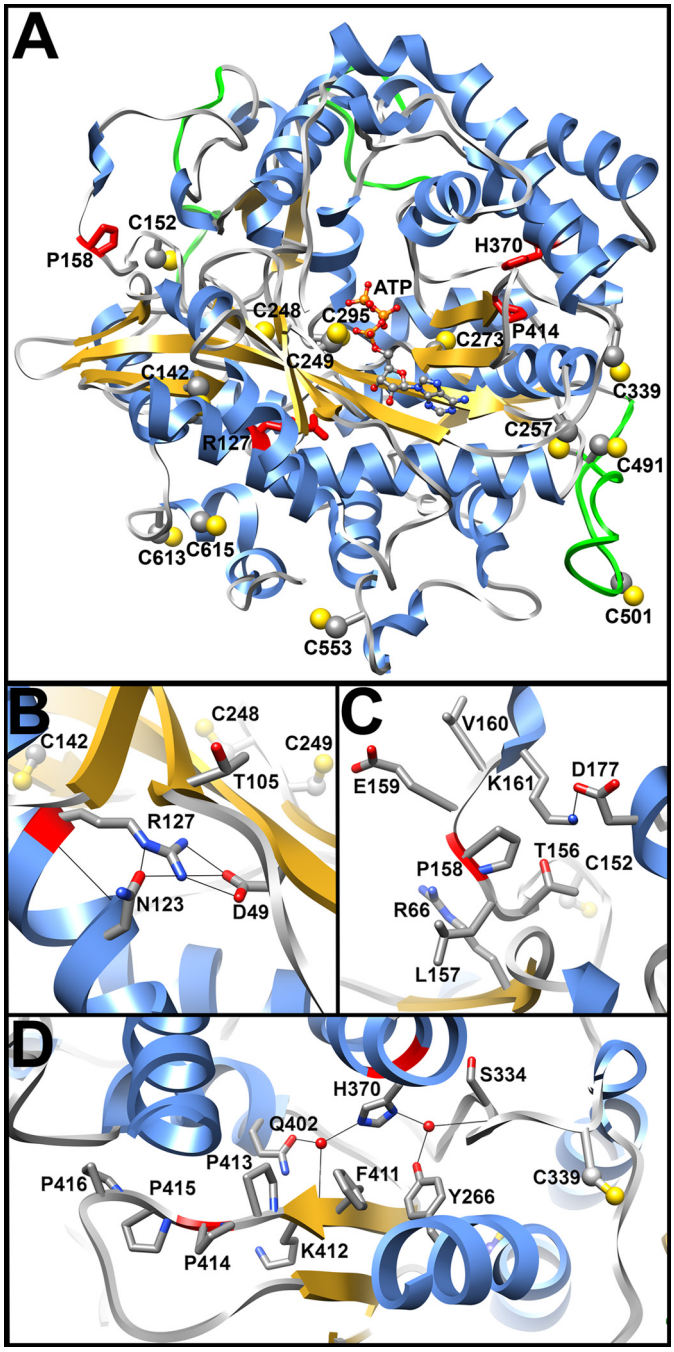

FIGURE 4. **Homology modeling of human glutamate cysteine ligase.** The folded structure of hGCLC was modeled with PDBViewer software package using the determined ScGCL structure. *Panel A*, the overall structure of hGCLC is shown in *ribbon* representation with β-strands colored in *yellow*, α-helices in *blue*, and loop regions in *gray*. Areas with low sequence identity to ScGCL are highlighted in *green* and represent regions of low model confidence. Cysteine residues are shown in *ball and stick* representation and amino acid residues with associated clinical mutations are colored in *red*. For reference, ATP was also docked within the model. *Panel B*, R127C mutation would disrupt a critical structural salt bridge between Arg-127 and Asp-49 and negatively impact the active site architecture. *Panel C*, Pro-158 is located in a loop region on the surface of hGCLC. Substitution with a leucine residue may disorder this loop, potentially impacting interactions with the modifier subunit. *Panel D*, both His-370 and Pro-414 are in close proximately to a β-strand containing Lys-412, which, based on comparison to ScGCL, is likely involved in orienting the β-phosphate of ATP. The H370L mutation would likely lead to the loss of two ordered water molecules which form hydrogen bonds that stabilize this region of the structure. Similarly, P414L would disrupt this region of the protein and negatively impact ATP binding.

Mg^{2+} and cysteine were already bound, arguing against a truly random binding of substrates. The ScGCL structures are consistent with an earlier study of bovine lenticular GCL, which suggested that glutamate (or glutamate and Mg^{2+} at the M1 site) is the first substrate to bind (51). Detailed kinetic studies of ScGCL to establish its precise mechanism are needed to resolve these inconsistencies.

The chemical reaction catalyzed by GCL involves two distinct steps. The glutamate γ-carboxylate, which is coordinated to the M1 Mg^{2+}, is oriented for an in-line attack of the γ-phosphate of ATP (52), which is positioned optimally by the three bound Mg^{2+} ions (Fig. 3*B*) as well as Lys-451 (Fig. 3*A*). The resulting γ-glutamylphosphate intermediate is susceptible to nucleophilic attack by the α-amino group of L-cysteine (20, 49), which may be activated by Glu-96 (40). Furthermore, structural data and mutagenesis studies support a role for a conserved arginine residue, Arg-472, in peptide bond formation, which may stabilize the developing negative charge on the tetrahedral transition state (44). Binding of the M1 Mg^{2+}, which contributes to the glutamate substrate site, is ATP-independent, whereas binding of the M2 and M3 Mg^{2+} ions requires the presence of ATP, consistent with previous mutagenesis studies of *T. brucei* GCL (40).

Homology modeling of the catalytic subunit of hGCL highlights cysteine residues that may be important for post-translational regulation. hGCL is a heterodimer comprised of a catalytic subunit that catalyzes formation of γ-glutamylcysteine and a modifier subunit, that increases the overall rate of product formation (30, 53). The heterodimer is stabilized by an intersubunit disulfide bond that may couple glutathione biosynthesis with the redox state of the cell (30, 54). However, recent work with mouse and *Drosophila* homologues suggests that an intermolecular disulfide bond is not required for complex formation and allosteric activation (48, 55).

Mutagenesis studies of hGCLC cysteine residues showed that one of its 14 cysteines (Cys-553) affects enzymatic activity (47). However, the subunits were still able to form the heterodimer, suggesting that noncovalent interactions are also important for holoenzyme formation. Examination of the hGCLC model indicates that Cys-553 is located in a surface exposed loop and may be involved in intersubunit interactions. Three additional cysteine residues, Cys-339, Cys-491, and Cys-501, map to similar mobile surface loops of the hGCLC model (Fig. 4*A*). The loop containing residues 490–507 is absent in the monomeric ScGCL, suggesting it may be a site of interaction with the human modifier subunit. Systematic studies are required to directly test the significance of each of these cysteine residues with respect to intersubunit interactions.

Hereditary disorder of hGCL is a rare autosomal recessive disease reported in 8 unrelated cases (15, 41, 42, 56–58), and is associated with low glutathione level in erythrocytes, markedly decreased GCL activity, hemolytic anemia, jaundice, and in some cases, progressive neurological disorders. Four single nucleotide mutations have been reported in hGCL deficiency, each leading to amino acid substitutions within the catalytic subunit of the enzyme: R127C, P158L, H370L, and P414L (15, 41, 42, 57). Shown in Fig. 4 are the locations of each of these four mutations in the hGCLC model. Although none are located

directly in the enzyme active site, these residues, as well as proximal residues, are highly conserved in higher eukaryotic GCL, including ScGCL. The exception is Pro-158. Analysis of the ScGCL structures and the hGCLC homology model suggests the molecular details of diminished catalytic activity.

Mutation of Arg-127 to a cysteine residue (Fig. 4*B*) would disrupt a salt bridge with Asp-49 and negatively impact the active site architecture. The backbone carbonyls of Asp-49 and Gly-48 contribute to the ATP binding site (similar to ScGCL in Fig. 3*A*) and Glu-50 is a critical catalytic residue. In addition, the Arg-127—Asp-49 salt bridge is adjacent to a loop containing Thr-105 and Pro-106 (Fig. 4*B*), which also contributes to formation of the ATP binding site. Thus, the introduction of disorder in this region by this substitution would negatively impact catalytic efficiency.

Pro-158 is located in a surface exposed loop found in both human GCLC and ScGCL, far removed from the enzyme active site (Fig. 4*C*). This region exhibits poor sequence conservation, with an isoleucine residue, Ile-170, at the equivalent position in ScGCL. As such, it is difficult to fully explain the phenotype associated with the P158L substitution. Perhaps the loop containing Pro-158 is involved in binding of the regulatory subunit in the heterodimeric human enzyme. However, other regions are also likely involved, since the modifier subunit can still interact with the P158L mutant (48). Interestingly, Ile-170 in ScGCL is in close proximity to Cys-70, a potential site of oxidation (supplemental Fig. S2), suggesting that this region may generally be involved in post-translational regulation.

Inspection of the human GCLC model suggests that both the H370L and P414L mutations are structurally disruptive (Fig. 4*D*). His-370 forms hydrogen bonds with two bound water molecules, which are needed to stabilize the β-strand containing Lys-412. Similarly, Pro-414 is located in a four-proline stretch in the loop immediately following this same β-strand. The reduced enzymatic activity observed in these two mutants is likely the result of impaired ATP binding, as Lys-412 is equivalent to Lys-451 in ScGCL (Fig. 3*A*). In ScGCL, this lysine interacts via bridging water molecules with the β-phosphate of bound ADP. Further kinetic characterizations of the point mutants to confirm this assertion are needed as previous studies did not report $K_{m(\mathrm{ATP})}$ values for either enzyme (15, 42).

In summary, the reported complexes of ScGCL provide considerable insight into substrate recognition, the role of Mg^{2+} in the enzyme-catalyzed reaction, and the overall catalytic mechanism. The prominent locations of several conserved cysteine residues indicate that post-translational modifications may be important in the regulation of enzymatic activity. Furthermore, the ScGCL structures allowed for the generation of a reasonable homology model of the human enzyme. Analysis of the ScGCL structures and hGCLC model explains the molecular basis of glutathione deficiency, resulting from clinically observed mutations in this enzyme. Furthermore, the results of these studies may assist in the design of novel therapeutics that modulate intracellular glutathione levels.

Acknowledgments—We thank the BioCARS staff for assistance in x-ray data collection, Dr. Mark Wilson (University of Nebraska) for helpful discussions, and Dr. Melanie Simpson (University of Nebraska) for thoughtful insights and review of the manuscript. We acknowledge Brandi Sommer for preparation of the ScGCL expression construct. Use of the Advanced Photon Source was supported by the United States Department of Energy, Basic Energy Sciences, Office of Science (Contract No. W-31-109-Eng-38). Use of BioCARS Sector 14 was supported by the National Institutes of Health, National Center for Research Resources (RR07707).

REFERENCES

1. Anderson, M. E. (1998) *Chem. Biol. Interact.* **111–112,[r] 1–14**
2. Higashi, T., Tateishi, N., Naruse, A., and Sakamoto, Y. (1977) *J. Biochem.* **82,** 117–124
3. Tateishi, N., Higashi, T., Naruse, A., Nakashima, K., and Shiozaki, H. (1977) *J. Nutr.* **107,** 51–60
4. Nicholson, D. W., Ali, A., Klemba, M. W., Munday, N. A., Zamboni, R. J., and Ford-Hutchinson, A. W. (1992) *J. Biol. Chem.* **267,** 17849–17857
5. Christ-Hazelhof, E., Nugteren, D. H., and Van Dorp, D. A. (1976) *Biochim. Biophys. Acta* **450,** 450–461
6. Lu, S. C. (1999) *FASEB J.* **13,** 1169–1183
7. Klatt, P., and Lamas, S. (2000) *Eur. J. Biochem.* **267,** 4928–4944
8. Buhl, R., Jaffe, H. A., Holroyd, K. J., Wells, F. B., Mastrangeli, A., Saltini, C., Cantin, A. M., and Crystal, R. G. (1989) *Lancet* **2,** 1294–1298
9. Staal, F. J., Roederer, M., and Herzenberg, L. A. (1990) *Proc. Natl. Acad. Sci. U.S.A.* **87,** 9943–9947
10. Sofic, E., Lange, K. W., Jellinger, K., and Riederer, P. (1992) *Neurosci. Lett.* **142,** 128–130
11. Andersen, J. K., Mo, J. Q., Hom, D. G., Lee, F. Y., Harnish, P., Hamill, R. W., and McNeill, T. H. (1996) *J. Neurochem.* **67,** 2164–2171
12. Townsend, D. M., Tew, K. D., and Tapiero, H. (2003) *Biomed. Pharmacother.* **57,** 145–155
13. Huynh, T. T., Huynh, V. T., Harmon, M. A., and Phillips, M. A. (2003) *J. Biol. Chem.* **278,** 39794–39800
14. Walsh, A. C., Li, W., Rosen, D. R., and Lawrence, D. A. (1996) *Cytogenet. Cell Genet.* **75,** 14–16
15. Beutler, E., Gelbart, T., Kondo, T., and Matsunaga, A. T. (1999) *Blood* **94,** 2890–2894
16. Gysin, R., Kraftsik, R., Sandell, J., Bovet, P., Chappuis, C., Conus, P., Deppen, P., Preisig, M., Ruiz, V., Steullet, P., Tosic, M., Werge, T., Cuénod, M., and Do, K. Q. (2007) *Proc. Natl. Acad. Sci. U.S.A.* **104,** 16621–16626
17. Griffith, O. W., and Mulcahy, R. T. (1999) *Adv. Enzymol. Relat. Areas Mol. Biol.* **73,** 209–267, xii
18. Strumeyer, D. H., and Bloch, K. (1960) *J. Biol. Chem.* **235,** PC27
19. Orlowski, M., and Meister, A. (1971) *J. Biol. Chem.* **246,** 7095–7105
20. Yip, B., and Rudolph, F. B. (1976) *J. Biol. Chem.* **251,** 3563–3568
21. Tateishi, N., Higashi, T., Shinya, S., Naruse, A., and Sakamoto, Y. (1974) *J. Biochem.* **75,** 93–103
22. Richman, P. G., and Meister, A. (1975) *J. Biol. Chem.* **250,** 1422–1426
23. Lu, S. C. (2009) *Mol. Aspects Med.* **30,** 42–59
24. Copley, S. D., and Dhillon, J. K. (2002) *Genome Biol.* **3,** research0025
25. Hibi, T., Nii, H., Nakatsu, T., Kimura, A., Kato, H., Hiratake, J., and Oda, J. (2004) *Proc. Natl. Acad. Sci. U.S.A.* **101,** 15052–15057
26. Hothorn, M., Wachter, A., Gromes, R., Stuwe, T., Rausch, T., and Scheffzek, K. (2006) *J. Biol. Chem.* **281,** 27557–27565
27. Ohtake, Y., and Yabuuchi, S. (1991) *Yeast* **7,** 953–961
28. Ghaemmaghami, S., Huh, W. K., Bower, K., Howson, R. W., Belle, A., Dephoure, N., O'Shea, E. K., and Weissman, J. S. (2003) *Nature* **425,** 737–741
29. Gill, S. C., and von Hippel, P. H. (1989) *Anal. Biochem.* **182,** 319–326
30. Huang, C. S., Chang, L. S., Anderson, M. E., and Meister, A. (1993) *J. Biol. Chem.* **268,** 19675–19680
31. Rodgers, D. W. (1994) *Structure* **2,** 1135–1140
32. Otwinowski, Z., and Minor, W. (1997) *Methods Enzymol.* **276,** 307–326

33. Adams, P. D., Grosse-Kunstleve, R. W., Hung, L. W., Ioerger, T. R., McCoy, A. J., Moriarty, N. W., Read, R. J., Sacchettini, J. C., Sauter, N. K., and Terwilliger, T. C. (2002) *Acta Crystallogr. D Biol. Crystallogr.* **58,** 1948–1954
34. Emsley, P., and Cowtan, K. (2004) *Acta Crystallogr. D Biol. Crystallogr.* **60,** 2126–2132
35. Murshudov, G. N., Vagin, A. A., and Dodson, E. J. (1997) *Acta Crystallogr. D Biol. Crystallogr.* **53,** 240–255
36. Davis, I. W., Leaver-Fay, A., Chen, V. B., Block, J. N., Kapral, G. J., Wang, X., Murray, L. W., Arendall, W. B., 3rd, Snoeyink, J., Richardson, J. S., and Richardson, D. C. (2007) *Nucleic Acids Res.* **35,** W375–W383
37. Pettersen, E. F., Goddard, T. D., Huang, C. C., Couch, G. S., Greenblatt, D. M., Meng, E. C., and Ferrin, T. E. (2004) *J. Comput. Chem.* **25,** 1605–1612
38. Ochi, T. (1996) *Toxicology* **112,** 45–55
39. Ochi, T. (1995) *Arch. Toxicol.* **70,** 96–103
40. Abbott, J. J., Pei, J., Ford, J. L., Qi, Y., Grishin, V. N., Pitcher, L. A., Phillips, M. A., and Grishin, N. V. (2001) *J. Biol. Chem.* **276,** 42099–42107
41. Hamilton, D., Wu, J. H., Alaoui-Jamali, M., and Batist, G. (2003) *Blood* **102,** 725–730
42. Mañú Pereira, M., Gelbart, T., Ristoff, E., Crain, K. C., Bergua, J. M., López Lafuente, A., Kalko, S. G., Garcia Mateos, E., Beutler, E., and Vives Corrons, J. L. (2007) *Haematologica* **92,** e102–e105
43. Guex, N., and Peitsch, M. C. (1997) *Electrophoresis* **18,** 2714–2723
44. Abbott, J. J., Ford, J. L., and Phillips, M. A. (2002) *Biochemistry* **41,** 2741–2750
45. Huang, C. S., Moore, W. R., and Meister, A. (1988) *Proc. Natl. Acad. Sci. U.S.A.* **85,** 2464–2468
46. Brekken, D. L., and Phillips, M. A. (1998) *J. Biol. Chem.* **273,** 26317–26322
47. Tu, Z., and Anders, M. W. (1998) *Biochem. J.* **336,** 675–680
48. Yang, Y., Chen, Y., Johansson, E., Schneider, S. N., Shertzer, H. G., Nebert, D. W., and Dalton, T. P. (2007) *Biochem. Pharmacol.* **74,** 372–381
49. Schandle, V. B., and Rudolph, F. B. (1981) *J. Biol. Chem.* **256,** 7590–7594
50. Jez, J. M., Cahoon, R. E., and Chen, S. (2004) *J. Biol. Chem.* **279,** 33463–33470
51. van Buskirk, G. E., Gander, J. E., and Rathbun, W. B. (1978) *Eur. J. Biochem.* **85,** 589–597
52. Matte, A., Tari, L. W., and Delbaere, L. T. (1998) *Structure* **6,** 413–419
53. Huang, C. S., Anderson, M. E., and Meister, A. (1993) *J. Biol. Chem.* **268,** 20578–20583
54. Seelig, G. F., Simondsen, R. P., and Meister, A. (1984) *J. Biol. Chem.* **259,** 9345–9347
55. Fraser, J. A., Kansagra, P., Kotecki, C., Saunders, R. D., and McLellan, L. I. (2003) *J. Biol. Chem.* **278,** 46369–46377
56. Beutler, E., Moroose, R., Kramer, L., Gelbart, T., and Forman, L. (1990) *Blood* **75,** 271–273
57. Ristoff, E., Augustson, C., Geissler, J., de Rijk, T., Carlsson, K., Luo, J. L., Andersson, K., Weening, R. S., van Zwieten, R., Larsson, A., and Roos, D. (2000) *Blood* **95,** 2193–2196
58. Hirono, A., Iyori, H., Sekine, I., Ueyama, J., Chiba, H., Kanno, H., Fujii, H., and Miwa, S. (1996) *Blood* **87,** 2071–2074

Supplemental data.

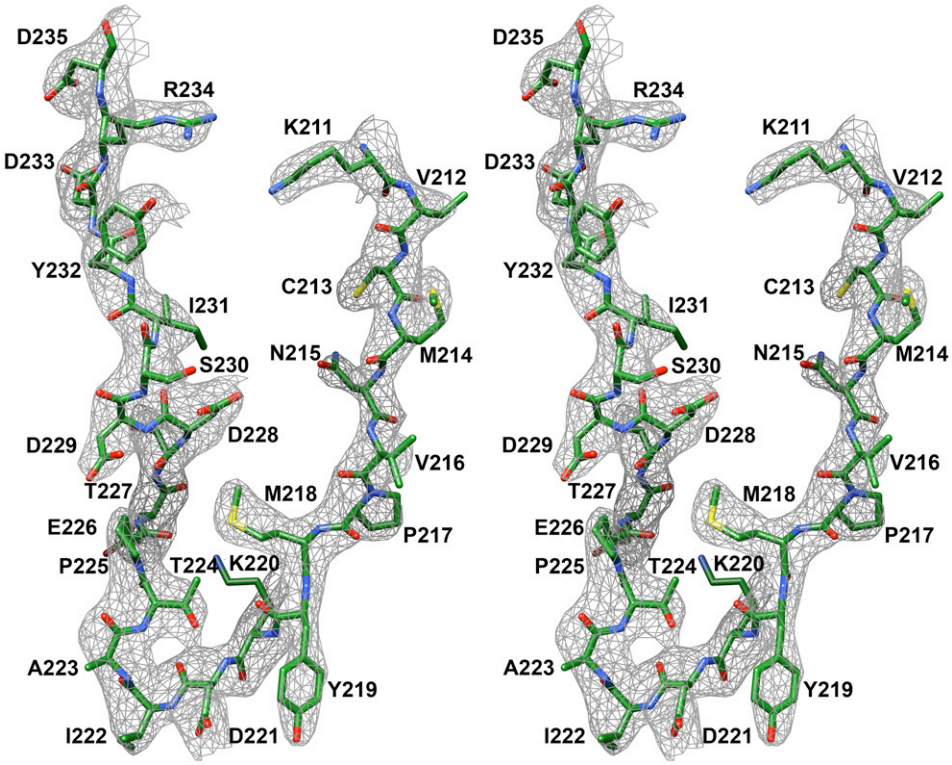

Supplemental Figure 1. Representative experimentally phased electron density map. The positions of 1 lead and 22 sulfur atoms were identified using the PHENIX software suite and used to calculate initial phase information. In the stereodiagram, the resulting electron density map following density modification is shown in grey and is contoured at 1 σ. The final ScGCL model corresponding to this region of the map is shown in stick representation with carbon atoms colored in green, oxygen in red, nitrogen in blue, and sulfur in yellow.

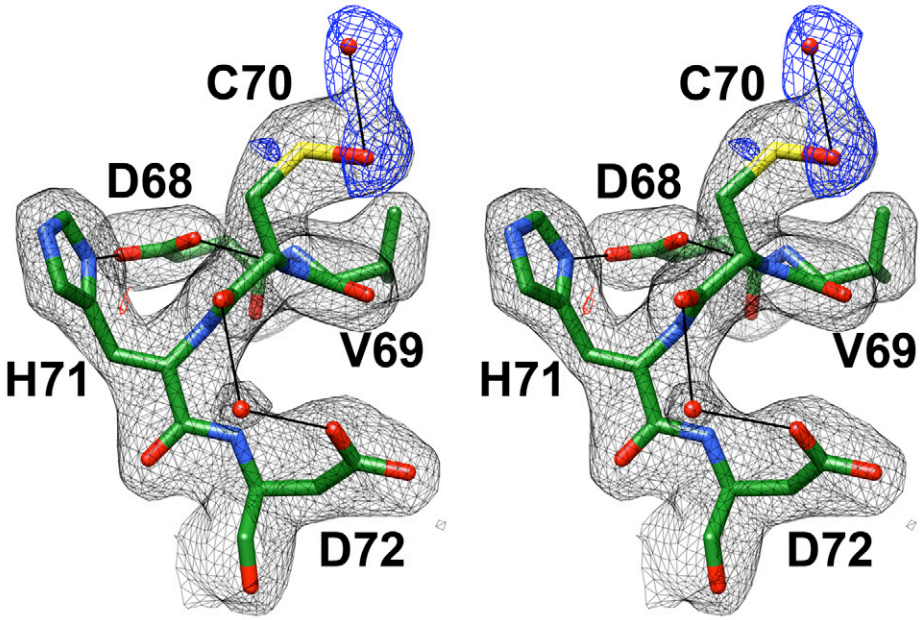

Supplemental Figure 2. Cysteine70 of ScGCL is oxidized to sulfenic acid in the ScGCL/Glu/Mg^{2+} complex. In the stereodiagram, the amino acid residues in close proximity to Cys70 are shown in stick representation and atoms are colored as in Supplemental Figure 1. Also shown are the calculated electron density maps after several rounds of refinement, but prior to inclusion of sulfenic acid oxygen in the model. The relevant $2F_o$-F_c electron density is contoured at 1.0 σ and illustrated in grey. Positive and negative peaks in the difference map, contoured at 3.0 σ, are shown in blue and red respectively. Potential hydrogen bonds were identified with Chimera and are indicated as solid black lines.